CAMBRIDGE
UNIVERSITY PRESS

Unsupervised clustering identifies thermohaline staircases in the Canada Basin of the Arctic Ocean

Mikhail G. Schee[1] ⓘ, Erica Rosenblum[1,2] ⓘ, Jonathan M. Lilly[3] ⓘ and Nicolas Grisouard[1] ⓘ

[1]Department of Physics, University of Toronto, Toronto, ON, Canada
[2]Centre for Earth Observation Science, University of Manitoba, Winnipeg, MB, Canada
[3]Planetary Science Institute, Tucson, AZ, USA
Corresponding author: Mikhail G. Schee; Email: mikhail.schee@alumni.utoronto.ca

Abstract

Thermohaline staircases are a widespread stratification feature that impacts the vertical transport of heat and nutrients and are consistently observed throughout the Canada Basin of the Arctic Ocean. Observations of staircases from the same time period and geographic region form clusters in temperature-salinity (T–S) space. Here, for the first time, we use an automated clustering algorithm called the hierarchical density-based spatial clustering of applications with noise to detect and connect individual well-mixed staircase layers across profiles from ice-tethered profilers. Our application only requires an estimate of the typical layer thickness and expected salinity range of staircases. We compare this method to two previous studies that used different approaches to detect layers and reproduce several results, including the mean lateral density ratio R_L and that the difference in salinity between neighboring layers is a magnitude larger than the salinity variance within a layer. We find that we can accurately and automatically track individual layers in coherent staircases across time and space between different profiles. In evaluating the algorithm's performance, we find evidence of different physical features, namely splitting or merging layers and remnant intrusions. Further, we find a dependence of R_L on pressure, whereas previous studies have reported constant R_L. Our results demonstrate that clustering algorithms are an effective and parsimonious method of identifying staircases in ocean profile data.

Impact Statement

Clustering algorithms are unsupervised machine learning methods that are used across many areas of data science. The use of such methods can automate the identification of certain features, thus allowing for the analysis of very large datasets. Here, we show that a particular clustering algorithm called hierarchical density-based spatial clustering of applications with noise (HDBSCAN) can be used to automatically identify thermohaline staircases in hydrographic profiles from the Arctic Ocean. Compared to previous detection methods, HDBSCAN has the advantages of requiring minimal prior knowledge and of automatically connecting individual staircase "steps" across different hydrographic profiles. We expect that this method could be applied to many similar datasets, offering a straightforward way to identify and track layers in thermohaline staircases across the world's oceans.

1. Introduction

Thermohaline staircases, formed by differential diffusion rates of heat and salt, appear as a series of vertically well-mixed horizontal layers, each separated by thin, strongly stratified interfaces. These

structures have been observed throughout the world's oceans (van der Boog et al., 2021a) as well as in saline lakes (Newman, 1976), while related double-diffusive staircases are thought to occur in gas giants such as Jupiter and Saturn (André et al., 2017; Pontin et al., 2021). In particular, they are well known to occur in the Arctic Ocean (Timmermans et al., 2008; Lu et al., 2022; Ménesguen et al., 2022). Around 250 to 800 meters below the surface of the Arctic Ocean, there is a layer of water originating from the Atlantic, which is warmer and saltier than the topmost layer that is in contact with the sea ice above (Timmermans et al., 2008). The core of the Atlantic water (AW) is defined as the maximum subsurface temperature and is generally at a depth of 400 m in the Canada Basin. Above this depth, in a region in which both temperature and salinity increase downwards, lie the lower halocline waters (LHW), where the staircases are found (Lu et al., 2022).

Two-thirds of the world's oceans are *alpha* oceans, which are stratified by temperature, with the warmest waters at the surface and colder waters at depth (Stewart and Haine, 2016). This is in contrast to the 15% that are *beta* oceans, the only regions where sea ice can form over deep water, such as the Arctic, which are primarily stratified by salinity, and therefore, the warm, salty AW is stable at depth (Carmack, 2007). The remaining oceans are called "transition zone oceans" (Stewart and Haine, 2016). While Arctic sea ice has been steadily disappearing (Comiso et al., 2008), the density stratification above the AW core has historically been strong enough to insulate surface waters from the warmth at depth (Shibley et al., 2017). However, the lower sections of Arctic staircases have been disappearing in recent years (Ménesguen et al., 2022). Many works have noted that the AW contains enough heat to melt all Arctic sea ice, if it were somehow able to reach the surface (Maykut and Untersteiner, 1971; Turner, 2010; Stranne et al., 2017; Shibley et al., 2020). Given their potential role in modulating the Arctic climate, it is important to be able to accurately identify thermohaline staircases in observations to monitor changes.

The first recorded observation of thermohaline staircases in the Arctic Ocean was made in 1969 at Ice Island T-3 (Neal et al., 1969). This iceberg, located somewhat northeast of the Canada Basin (often defined as 72–84°N, 130–155°W, see, e.g., Peralta-Ferriz and Woodgate, 2015), was the site of dozens of hydrographic profiles that contain clearly visible staircases (Neshyba et al., 1971, 1972; Neal and Neshyba, 1973). Subsequent observations indicate that the staircases have been a consistent feature of the Canada Basin, including from data collected during the Arctic Internal Wave Experiment (AIWEX) (Padman and Dillon, 1987, 1988, 1989) and the Surface Heat Budget of the Arctic (SHEBA) experiment (Shaw and Stanton, 2014). The frequency of such observations increased dramatically in 2004, when the introduction of autonomous ice-tethered profilers (ITPs) made possible the continuous, year-round sampling of the Arctic Ocean water column (Toole et al., 2011).

Although many early studies identified staircases by visual inspection, the recent increase in available data has spurred researchers to turn to algorithmic approaches. Here, we detail several previous studies whose foundational work was critical in the development of the current study. All of these studies used a similar approach to detect data points that fall within some well-mixed layer (henceforth for brevity simply "layer") on a profile-by-profile basis. Timmermans et al. (2008) defined a point in a hydrographic profile to be detected within a layer when the local vertical potential temperature gradient $\partial\theta/\partial z$ is below $0.005\,°\text{C}\,\text{m}^{-1}$, roughly an order of magnitude smaller than the overall gradient for a typical profile. Shibley et al. (2017) extended the automated detection method of Timmermans et al. (2008) by including two additional conditions: (1) For each experiment, they visually determined different threshold values on both $\partial\theta/\partial z$ and on the temperature difference between neighboring points and (2) after then running the detection method, those authors only considered staircases that consisted of at least three layers. van der Boog et al. (2021b) developed a similar staircase detection algorithm, but chose threshold values of vertical density gradients that were expected to be applicable to staircases in all of the world's oceans, not just the Arctic. Specifically, they set a vertical gradient threshold of $\partial\sigma_1/\partial p \leq 0.0005\,\text{kgm}^{-3}\,\text{dbar}^{-1}$, where σ_1 is the density anomaly referenced to 1000 dbar. Then, from the subset of data that meets that condition, only mixed layers with a maximum variation of density anomaly of $0.005\,\text{kgm}^{-3}$ or less, and whose neighboring interfaces had thicknesses of 30 dbar or less, were considered. Lu et al. (2022) defined the intersections between layers and interfaces as locations where the difference in the potential

temperature gradient between two neighboring points is greater than $0.003 \,^{\circ}\mathrm{C\,m^{-1}}$, then disregarded the points within the interfaces. After performing this detection, Lu et al. (2022) then made cross-profile connections with the layer points that remained, following the work of Padman and Dillon (1988), and used valleys in histograms of salinity to guide their choice of boundaries between layers, some of which were manually adjusted. We find it useful to distinguish between these two steps: the detection of points within layers for each profile and the connection of these points to those in other profiles that are within the same layer. Many previous studies did not describe a connection method because it was not needed for their ends; we use this framing to call attention to the novel aspects of our contribution.

All of the above techniques first detect a subset of the data points that are likely within layers based on vertical gradient thresholds. This approach requires sufficient knowledge of the staircases properties to select appropriate thresholds, as well as data with sufficient vertical resolution to accurately estimate the gradients. The connection algorithm Lu et al. (2022) describe, after its completion, still requires some amount of manual intervention to produce a final dataset of staircase layers. A commonality of all of these approaches is that they are purpose-built for the task of detecting staircases in specific contexts. These factors motivate the search for a more general approach to detect and connect thermohaline layers across different profiles, which could offer advantages such as greater scalability and applicability as well as more ready reproducibility, all of which would accelerate the pace of research on these important structures.

Many studies, notably Timmermans et al. (2008), have observed that a collection of profiles that includes well-mixed layers, such as density staircases, is associated with clustered patterns when plotted in temperature-salinity (T–S) space (Schmitt et al., 1987; Toole et al., 2011; Yu et al., 2017; Bebieva and Timmermans, 2019). This clustering indicates that layers are thin sheets, extending laterally for hundreds of kilometers (Timmermans et al., 2008; Lu et al., 2022). These patterns occur where a staircase is present because all data points within a particular layer have approximately the same temperature and salinity values as other observations from the same layer, regardless of their vertical position within the layer. This fact suggests that staircases could be detected by directly identifying clusters in T–S space. Clustering algorithms are a type of unsupervised machine learning and have been previously used in a variety of different oceanographic applications (Sonnewald et al., 2021). Examples include grouping observations from freely drifting instruments in the Nordic Seas (Koszalka and LaCasce, 2010), studying surface wave variability in the North Atlantic (Espejo et al., 2014), classifying the heat content of hydrographic profiles (Maze et al., 2017), resolving trapping in mesoscale eddies (Ma et al., 2019), defining spatial regions for Southern Ocean temperature profiles (Jones et al., 2019), detecting ENSO events (Houghton and Wilson, 2020), finding hot spots for mixing in the Southern Ocean (Rosso et al., 2020), and identifying shifts in the North Atlantic circulation (Desbruyères et al., 2021). However, to the best of our knowledge, they have never before been used to identify thermohaline staircases.

Here, we apply a method based on the hierarchical density-based spatial clustering of applications with noise (HDBSCAN) algorithm (Campello et al., 2013) to both detect and connect thermohaline staircases across Arctic hydrographic profiles. This method has several advantages. It detects and automatically connects staircase layers across large hydrographic datasets in one step. In the past, HDBSCAN has been successfully applied to datasets with a number of points that were an order of magnitude larger than in this study, suggesting the application we present here could be scaled to accommodate more data (Logan and Fotopoulou, 2020). Also, it does not consider profiles individually and therefore, does not require that each profile have fine vertical resolution. Our implementation of this algorithm does require knowledge of the typical layer thickness and the expected global salinity range of the staircase; however, as we will show, this is a more flexible requirement compared to determining threshold gradients. Most importantly, it exhibits excellent performance producing a final, connected dataset of layers to which no subsequent adjustments need to be made, and is thus suitable for application to datasets with a large number of points as well as being more easily reproducible. The purpose of this paper is to present this method, and so we will note possible implications of our results but will not explore them in great detail.

The structure of this paper is as follows. First, in Section 2, we introduce and explain our choice of the datasets used in our analysis. In Section 3, we introduce HDBSCAN and describe how we use it to identify

staircases and how we choose the input parameters. Then, in Section 4, we apply this method to data from two different ITP experiments, focusing on results that reproduce those from the studies of Timmermans et al. (2008) and Lu et al. (2022), hereafter denoted as T08 and L22, respectively. Finally, in Section 5, we use the comparison between our results and those of T08 and L22 to evaluate the performance of the clustering algorithm and give recommendations on when and how it can be best used to identify staircases.

2. Data

ITPs are automated, vertically profiling instruments that are connected via a wire cable to a surface buoy on an ice floe (Toole et al., 2011). The wire extends from the surface, through the ice, down to depths of 500–800 m. The profiler travels up and down the wire roughly two to three times a day, collecting high-resolution (~25 cm) measurements of salinity, temperature, and pressure with a salinity precision of ± 0.005 g/kg and a temperature precision of $\pm 0.001\,°C$ (Timmermans et al., 2008; Shibley et al., 2017; Bebieva and Timmermans, 2019). Each traverse, alternating up or down, is recorded as a separate profile.

In this paper, data from two different ITP experiments, ITP2 and ITP3, are analyzed; see Table 1 for a summary. Because the measuring instruments are located at the top of the profiler, we use only the up-going profiles in order to avoid the known distortion caused by the wake of the profiling unit in the down-going profiles (Shibley et al., 2017). Figure 1 shows the locations of all up-going profiles for each of the two ITP experiments. We choose to analyze ITP2 and ITP3, in particular, to reproduce several results of T08 and L22, respectively.

Table 1. Details of the ice-tethered profilers (ITPs) used in this study

ITP	Start date	Days in operation	Starting position	Along-path distance (km)	Longest span[a] (km)	Total profiles	Up-going profiles
2	August 19, 2004	40	77° 10.4'N, 141° 13.0'W	390	191	242	121
3	August 23, 2005	382	77° 36.1'N, 142° 11.8'W	2541	441	1531	766

[a]The maximum distance between any two, not necessarily consecutive, profiles.
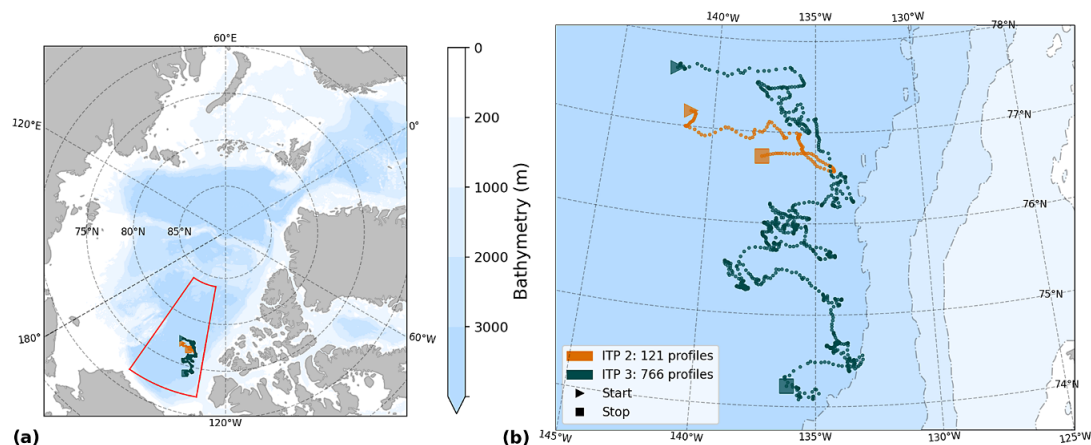

(a)   (b)

Figure 1. A map showing the locations of all profiles used from ITPs 2 and 3, showing the whole Arctic in (a) and a zoomed-in view in (b). The red box designates the Canada Basin as defined by Peralta-Ferriz and Woodgate (2015).

At this point, we note some choices in the study relative to those of T08 and L22. Here, we choose to work with pressure, a directly measured quantity, while both of those studies use depth, which is derived from pressure; as the conversion between pressure and depth is linear, this difference does not affect our results or comparisons. Also note that although both of those earlier studies use potential temperature θ, we choose instead to use conservative temperature Θ, as recommended by TEOS-10 (McDougall and Barker, 2011). For the range of temperatures and salinities in the data we analyze, the difference $|\theta - \Theta|$ is a systematic shift that is always less than 0.05 °C. Because this shift is relatively constant, our results are not sensitive to this choice. Furthermore, TEOS-10 recommends using absolute salinity S_A over practical salinity S_P. Our results do not change significantly using one versus the other (see Supplementary Material), so we choose to use S_P to make direct comparisons to the salinity ranges used by T08 and L22.

Staircases are only found in certain vertical ranges of the water column. However, as noted by L22, the salinity values of the layers are much more consistent across different profiles than their pressure or temperature characteristics, so we focus our analyses on a specific salinity range for each ITP. An appropriate range can be estimated by inspection of a few individual profiles or from general knowledge of the salinity range of staircases in the region. The bounds of this range need not be precise, but choosing a range that is too small will potentially miss layers. Running the algorithm on a liberally large range to capture all potential layers will take longer and may also return some clusters that do not correspond to meaningful thermohaline staircase layers. However, in Section 3.3, we detail a process of identifying erroneous clusters. For easier comparison, we choose salinity ranges used in past work, namely, 34.05–34.75 g/kg for ITP2 following T08 and 34.21–34.82 g/kg for ITP3 following L22.

As discussed in more detail below, the clustering algorithm does not distinguish between the different times and locations at which different profiles were taken. It follows that a dataset to be analyzed should not span larger temporal or spatial scales than the scales the staircases are known to be coherent across. T08, who analyzed much of the same data we do, found staircases that spanned the entire Canada Basin (approximately 800 km) and lasted at least 2 years. We define the longest span as the maximum distance between any two, not necessarily consecutive, profiles. We find the longest span (≤ 441 km) and duration (≤ 382 days) of the two ITPs we analyzed (see Table 1) are indeed smaller than the expected staircase coherence scales.

3. Methods

3.1. The HDBSCAN clustering algorithm

To identify T–S clusters as evidence for staircases within the ITP data, we use the HDBSCAN algorithm, which clusters data based on the relative densities in different regions. Algorithm-identified clusters in the ITP data are expected to correspond to staircase layers, with some exceptions, as detailed in Section 3.3. While Campello et al. (2013) present the algorithm in full detail, here we briefly review its general principles.

In the context of density-based clustering algorithms, the term "density" refers to a measure of the relative number of data points in a certain region of parameter space. HDBSCAN estimates the density of a region based on the distances between points and a number of their nearest neighbors, creating a hierarchy of clusterings from which it chooses the most prominent. First, it calculates the "core distance" ε for each point as the minimum radius of a circle needed to encompass its m_{pts} nearest neighbors. The inverse of ε represents density; when it is small, points are close together and when it is large, points are spread out. HDBSCAN then creates a hierarchy of clusterings, starting with the largest ε and working down. For each value ε_0, it first detects the level-set of non-noise points, where $\varepsilon \leq \varepsilon_0$, then connects points together in the same cluster if they are within a distance of ε.

As the value of ε_0 decreases, a particular cluster may change by shrinking, splitting, or disappearing entirely. Having built this hierarchy tree, HDBSCAN can then select clusters at the ends of branches even though different branches may terminate at very different values of ε_0. However, when the data are

particularly noisy, just before crossing the ε_0 threshold where a cluster would disappear, it may split into many small, spurious clusters. To avoid including these artifacts in the final result, the algorithm ignores all clusters with fewer than m_{clSize} number of points. The recommendation of the authors of HDBSCAN and the default behavior of the "hdbscan" Python package is to set $m_{clSize} = m_{pts}$ (Campello et al., 2013; Moulavi et al., 2014), giving one input parameter which controls both how the core distance is calculated and the minimum points per cluster. While there are other optional input parameters for HDBSCAN (see Supplementary Material), the results we obtained using the default settings were satisfactory, so we did not investigate their effects.

We choose HDBSCAN over other types of clustering algorithms for several reasons. Many previous oceanographic studies used partitioning algorithms such as k-means (Koszalka and LaCasce, 2010; Espejo et al., 2014; Houghton and Wilson, 2020) or Gaussian mixture models (Maze et al., 2017; Jones et al., 2019; Rosso et al., 2020; Desbruyères et al., 2021); however, partitioning algorithms require one to specify the number of clusters a priori, which is not known for our application. The first reason for choosing HDBSCAN is that it does not have this requirement (Ester et al., 1996; Jones et al., 2019). Second, HDBSCAN allows points that lie outside a cluster to be categorized as "noise." In our case, this is important because points in an interface between layers should not be assigned to any cluster. Third, unlike DBSCAN, which uses the same threshold ε_0 for all clusters throughout the domain (Ester et al., 1996; Campello et al., 2013), HDBSCAN creates a hierarchy of clusterings with different ε_0 and can, therefore, correctly identify clusters that vary significantly in both the number of points per cluster and the densities of points within the clusters (McInnes et al., 2017). Fourth, HDBSCAN can correctly identify arbitrarily shaped clusters, whereas partitioning algorithms like k-means generally find center-defined clusters, which, because points are assigned to clusters based on their distance from the cluster's center point, are only equipped to find globular or convex clusters (Ester et al., 1996; Hinneburg and Keim, 2003). This is important because the shapes of clusters associated with thermohaline staircases are not necessarily globular. Lastly, HDBSCAN requires only one input parameter (m_{pts}) to be specified, reducing the number of choices to be made before each run of the algorithm. Further, we determine the value of m_{pts} systematically, as explained below.

Having chosen a clustering algorithm, we now turn to specifying the two-dimensional space within which the clustering algorithm will operate. Figure 2(a) shows data from ITP2 in Θ–S_P space, where discrete groups of points associated with individual layers and spanning multiple profiles are apparent; these are colored according to their eventual partitioning into clusters. Note the occurrence of occasional gaps in Θ values, seen in the salinity ranges 34.16–34.30 and 34.65–34.74 g/kg. These result from the uneven spatial coverage of the meandering drift path of the ITPs (see Figure 1) together with the tendency for the temperature to vary more horizontally within a particular layer than salinity (Lu et al., 2022). In order to avoid HDBSCAN splitting such groups of points into multiple clusters for the same layer, for each temperature profile $\Theta(z)$, we define the local anomaly as

$$\Theta'(z) = \Theta(z) - \frac{1}{\ell} \int_{z-\ell/2}^{z+\ell/2} \Theta(z')dz', \tag{3.1}$$

where ℓ is the width of a rectangular moving average window. Presenting the ITP2 data in $\Theta' - S_P$ space rather than $\Theta - S_P$ space, as in Figure 2(c), leads to groups that are more centered around zero along the temperature axis, without notable gaps. We choose to work in this space as it will allow HDBSCAN to group points more accurately. We also confirmed the difference between using Θ or θ and S_P or S_A did not significantly affect the results. Finally, we mention that HDBSCAN is sensitive to the aspect ratio of the axes; however, because the results were found to be satisfactory, we did not investigate this dependency.

3.2. Selecting values of input parameters

It remains to choose values for the method parameters. The HDBSCAN algorithm is deterministic; that is, given the same arrangement of input data and the same value of the m_{pts} parameter, it will find the same clusters every time. The exact arrangement of data in $\Theta' - S_P$ space that we feed into the algorithm depends
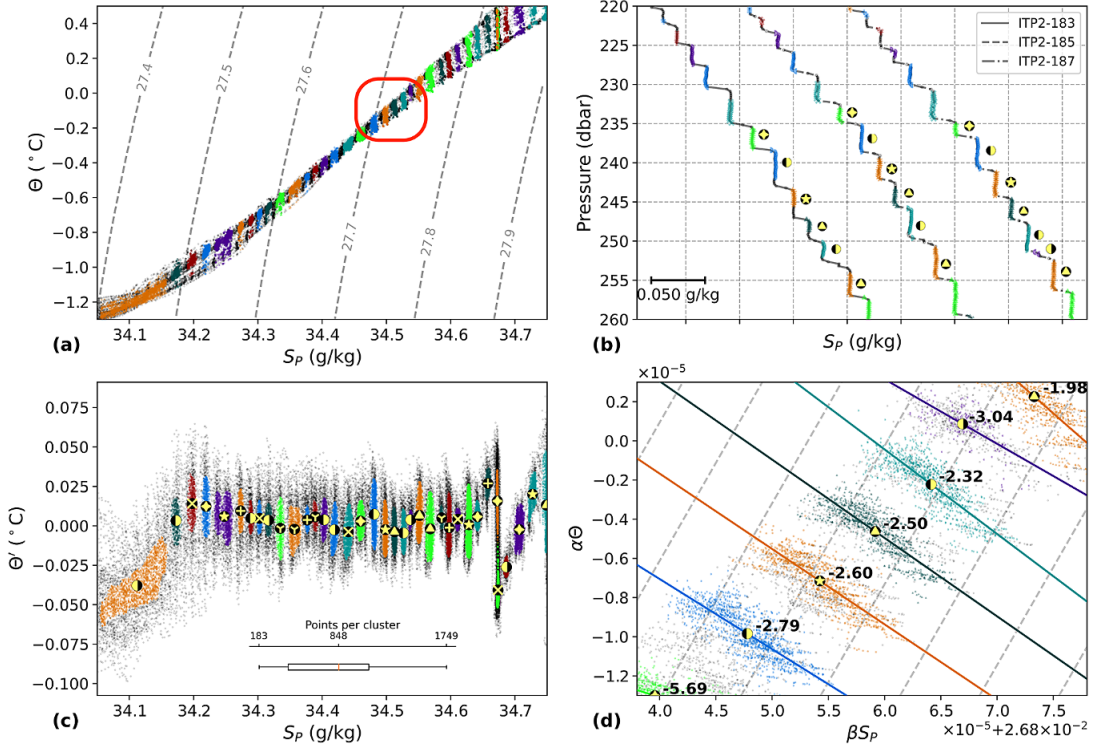
Figure 2. *Results from the clustering algorithm with $m_{pts} = 170$ and $\ell = 25$ dbar run on 53,042 data points in the salinity range 34.05–34.75 g/kg from all up-going ITP2 profiles. (a) The data in Θ–S_P space with dashed lines of constant potential density anomaly (kgm^{-3}) referenced to the surface. The red box bounds the clusters marked in panels (b) and (d). (b) Profiles 183, 185, and 187 from ITP2 in a limited pressure range to show detail. Each profile is offset in S_P for clarity. (c) The spatial arrangement used as input for the algorithm where the gray points are noise and each color-marker combination indicates a cluster. The same color-marker combinations are used in each panel, and the markers in panels (c) and (d) are at the cluster average for each axis. (d) A subset of the data in $\alpha\Theta$–βS_P space with the linear regression line and inverse slope (R_L) noted for each individual cluster and with dashed lines of slope $\alpha\Theta/\beta S_P = 1$.*

on three factors: (1) the set of profiles that we include, (2) the salinity range that we decide to analyze, and (3) the window width ℓ used to calculate the local anomaly of conservative temperature Θ' in Equation (3.1). We discussed our method of selecting the profiles and salinity range previously in Section 2. Here, we explain how we select values for ℓ and m_{pts}.

The results of a clustering algorithm can be judged on the basis of either external or internal validation. External validation methods involve comparing the clustering results to an external "ground truth," while internal validation methods use the data themselves to provide a measure of quality for the clustering (Moulavi et al., 2014). In this application, external validation would require detailed labeling, indicating to which layer, if any, each individual point belongs. Such labels could be determined by a separate method; however, we aim for this method to be broadly applicable to more than just reproducing previous results. Therefore, we tune our selection of ℓ and m_{pts} using density-based clustering validation (DBCV) (Moulavi et al., 2014) as an internal validation. DBCV considers good clustering solutions to be those in which the lowest-density regions within the clusters are still denser than the highest-density regions of the surrounding noise points. It bases the density estimates
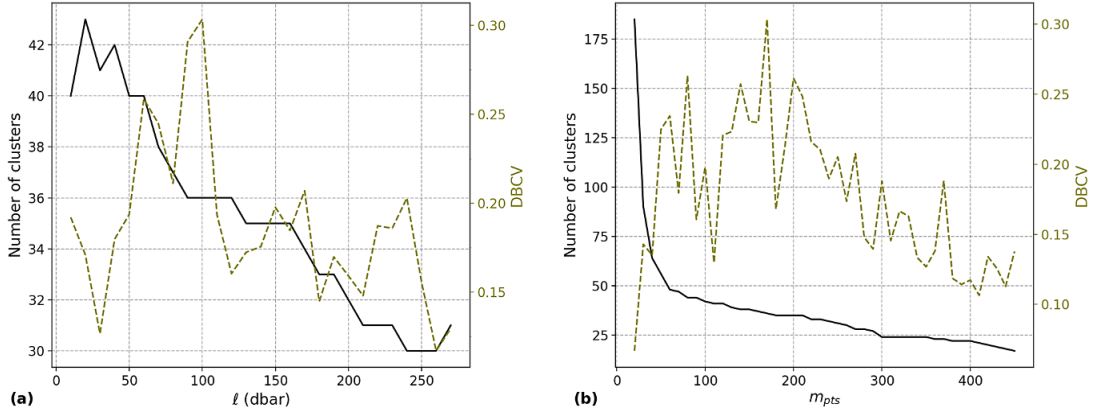
Figure 3. *A parameter sweep showing the number of clusters found (solid lines) and DBCV (dashed lines) in ITP2 as a function of (a) 27 different values of ℓ with $m_{pts} = 170$ and (b) 44 different values of m_{pts} with $\ell = 25$ dbar.*

on the so-called "mutual reachability distance," defined for each pair of points to be the maximum ε of either point or the distance between the two, whichever is largest. For more details, see Moulavi et al. (2014).

To evaluate algorithm performance, we performed a parameter sweep through different values of ℓ and m_{pts}, and present the number of clusters found together with the DBCV scores in Figure 3. For the ℓ dependence, see Figure 3(a), we find a downward trend in the number of clusters as ℓ increases. DBCV scores tend to be larger in the middle of the ℓ range, with the highest score occurring for $\ell = 25$ dbar. We may also note that the choice of ℓ shapes a large-scale feature of the Θ'–S_P plots. In Figure 2(c), a zig-zag pattern of increasing, rapidly decreasing, and then increasing again Θ' is seen in the range of $S_P \approx 34.63$–34.72 g/kg. This pattern is due to the presence of the AW subsurface temperature maximum in Θ profiles; it disappears when ℓ is small while becoming more exaggerated for larger ℓ (see Supplementary Material). Based upon previous studies of staircases in the Canada Basin during this time period (Timmermans et al., 2008; Lu et al., 2022), we estimated the typical layer thickness to be 5 m in height or 5 dbar in pressure, though we found similar results for estimates of 0.5–7.5 dbar (see Supplementary Material). The choice $\ell = 25$ dbar, where the largest DBCV score occurs, thus corresponds to approximately five times the typical layer thickness. This value is found to be large enough that the staircases are completely smoothed out yet small enough that the features outside the analyzed pressure range do not significantly affect the moving average.

We now turn to m_{pts}, which under the default settings of HDBSCAN, sets the minimum number of points in a cluster (Campello et al., 2013). If the value of m_{pts} is too small, the algorithm may erroneously split a cluster that represents one layer into multiple, smaller clusters, while a too-large value of m_{pts} would lead to the incorrect grouping of multiple discrete layers into a single cluster. Note that this upper bound on a reasonable m_{pts} depends greatly on the number of data points given to the algorithm the more data points the algorithm is given, the higher the value of m_{pts} can reasonably be set. In the parameter sweep of Figure 3(b), we find the number of clusters decreases rapidly until $m_{pts} \approx 60$, then decreases at a much slower rate, while the highest DBCV scores occur for intermediate values of m_{pts}. As with ℓ, we choose the value of m_{pts} having the highest DBCV score. For ITP2, this led to our selection of $m_{pts} = 170$.

Running HDBSCAN on ITP2 using the procedure outlined above with the choices $\ell = 100$ and $m_{pts} = 170$ leads to the clusters presented in Figure 2. Following the same parameter selection process for ITP3, we obtain the values $\ell = 25$ dbar and $m_{pts} = 580$ (see Supplementary Material). Table 2 summarizes our input parameter choices and the resulting number of clusters and DBCV values for both ITP2 and ITP3.

Table 2. *The values of parameters used to run the clustering algorithm over both datasets*

		Input parameters				Results	
ITP	Study to reproduce	Number of profiles	Salinity range (g/kg)	ℓ	m_{pts}	Number of clusters[1]	DBCV
2	Timmermans et al. (2008)	121	34.05–34.75	25 dbar	170	36 (31)	0.3034
3	Lu et al. (2022)	766	34.21–34.82	25 dbar	580	43 (40)	0.3862

[1]The first number is the total number of clusters found by the algorithm. The second is the number of clusters that were neither outliers in IR_{S_P} nor R_L.

3.3. Evaluating the clustering algorithm results

The DBCV score gives a measure of quality for the clusters in terms of their densities of points relative to the surrounding noise. However, DBCV does not take into account the properties of the clusters that we expect from the physical situation of staircases, such as their spans in Θ and S_P or how far they are from neighboring clusters. We, therefore, present two metrics to help predict whether each cluster will accurately represent what we expect from layers within staircases: the lateral density ratio R_L and the normalized inter-cluster range IR.

The relative strength of horizontal variations in salinity and temperature along the ith layer is described by the lateral density ratio

$$R_L^i = \frac{\beta \Delta S_P}{\alpha \Delta \Theta}, \tag{3.2}$$

where $\beta = \rho^{-1} \partial \rho / \partial S_P$ is the haline contraction coefficient, $\alpha = -\rho^{-1} \partial \rho / \partial \Theta$ is the thermal expansion coefficient, and ΔS_P and $\Delta \Theta$ are the variations in salinity and temperature, respectively, along a particular layer (Radko, 2013; Bebieva and Timmermans, 2019). We estimate R_L by finding the inverse slope of the best-fit line through each cluster in $\alpha \Theta$–βS_P space (see Figure 2(d)) (Chen, 1995; Timmermans et al., 2008). These lines are found using Orthogonal Distance Regression, which is more suitable than ordinary least squares in our case due to the presence of variability along both the $\alpha \Theta$ and βS_P axes (Winton, 2011); however, both methods yield similar results (not shown).

R_L quantifies the relative importance of S_P and Θ for the density of that layer (Timmermans et al., 2008; Bebieva and Timmermans, 2019) and is known to be directly related to the ratio of the vertical fluxes of salinity and heat within a staircase (Bebieva and Timmermans, 2019). Note that the lateral density ratio R_L is distinct from the density ratio, R_ρ, which is defined using the same Equation (3.2) but with ΔS_P and $\Delta \Theta$ taken in the vertical direction (Shibley et al., 2017). The relative constancy of R_L values across time and space has been interpreted as reflecting the remarkable degree of lateral coherence of staircase layers (Toole et al., 2011). The values of R_L have also been shown to be remarkably similar across neighboring layers (Timmermans et al., 2008). Therefore, if a value of R_L lies significantly outside of the general range of its neighbors, the cluster either reflects the erroneous grouping of multiple layers into a single cluster, or else a physical merging or splitting of layers, as discussed in Section 4.2.

We also define a measure of the relative spread of a variable, such as temperature or salinity, within a cluster in comparison with the differences between adjacent clusters. Ordering the clusters sequentially in density, the normalized inter-cluster range for the ith cluster is given by

$$IR_v^i = \frac{v_{max}^i - v_{min}^i}{\min\left(|\bar{v}^i - \bar{v}^{i-1}|, |\bar{v}^i - \bar{v}^{i+1}|\right)}, \tag{3.3}$$

where $i-1$ and $i+1$ denote the adjacent clusters to either side, v is the variable of interest (i.e., pressure, Θ, or S_P), v_{max}^i and v_{min}^i are the maximum and minimum values of the variable v within cluster i, and $\bar{v}^i$ denotes the mean value of v for cluster i. The numerator is the span between the maximum v_{max}^i and minimum v_{min}^i within cluster i. The denominator is the span between the mean of that cluster $\bar{v}^i$ and the

mean of either the cluster above or below, whichever is smaller. For clusters at either end of the variable space, we take the denominator to be the span between the mean of the ith cluster and that of its single neighbor.

The inter-cluster range IR_v, therefore, quantifies the range of a given variable, v, within a cluster in comparison with the range to the nearest neighboring cluster. For a staircase, the salinity values within one layer are generally well separated from the salinity values of the neighboring layers (Lu et al., 2022). Therefore, we expect that the clusters with large IR_{S_P} could represent a part of a single layer that was erroneously divided into multiple clusters by the algorithm or entirely different physical features, as discussed in Section 4.3.

In order to evaluate clusterings, we choose a method to detect outliers in both IR_{S_P} and R_L. We define outliers as points more than two standard deviations from the mean or equivalently with a z-score greater than 2 (approximately corresponding to a p-value of 0.05 for a two-tailed test). More sophisticated outlier detection methods exist, and while this approach is not guaranteed to find all erroneous clusters, outliers in IR_{S_P} and R_L give us an indication, based on simple and measurable physical characteristics, of particular clusters that may not represent a single, full layer and which therefore require closer inspection. Although such outliers could be manually adjusted to better capture single, complete layers, we disregard them when calculating statistics and trends.

4. Results

Now, having presented the HDBSCAN clustering algorithm, our process of selecting ℓ and m_{pts}, and metrics to identify erroneous clustering, we apply this method to data from ITP2 and ITP3.

4.1. Properties of detected layers

As a starting point, we examine the average value of pressure, Θ, or S_P for each cluster found from profiles collected by ITP3. Inspired by L22, we plot those values over time in Figure 4. We find that the clustering algorithm is capable of tracking individual layers across hundreds of profiles collected along the 2541 km-long track traced by ITP3 over 382 days. A pattern emerges where the pressures of individual layers appear to have more variability than temperature and salinity, consistent with T08. Moreover, we find that salinity variations within a layer are smaller than the salinity differences between two neighboring layers, while the opposite is true for pressure and temperature (similar to L22; see their Figure 3). We find similar results for ITP2 (see Supplementary Material).

More quantitatively, we find differences in salinity between clusters are approximately seven times larger than variations within a cluster. That is, we compute the standard deviation of salinity within each cluster and find that the median is 2.2 mg/kg, while the median absolute difference between the average salinity of adjacent clusters is 15.4 mg/kg. This is in agreement with L22, who found inter-layer salinity differences to be an order of magnitude larger than variations within a layer. Furthermore, the median normalized inter-cluster ranges (Equation (3.3)) in Table 3 quantitatively confirms the qualitative patterns noted by T08 and L22 as $\widehat{IR}_p, \widehat{IR}_\Theta > 1$ and $\widehat{IR}_{S_P} < 1$ for both ITPs, where $\widehat{}$ indicates the median. Table 3 also contains the median of the differences between neighboring cluster averages of temperature, $\widehat{\Delta\Theta}$, and salinity, $\widehat{\Delta S_P}$, for both ITPs. For ITP3, these values of 0.048 °C and 15.4 mg/kg match those of L22, which are 0.05 °C and 17 mg/kg. They also agree with T08, who reported the difference in temperature and salinity across interfaces to be $\delta\theta \approx 0.04\,°\mathrm{C}$ and $\delta S \approx 14$ mg/kg.

4.2. Outliers and splitting/merging layers

As discussed previously in Section 3.3, outliers have been identified in the inter-cluster salinity range IR_{S_P} as well as the lateral density ratio R_L. Figure 5 shows IR_{S_P} and R_L for both ITPs with outliers indicated by red circles. We find that these outliers can either be due to erroneous clustering or indicate the presence of different physical features, such as the splitting or merging of thermohaline staircase
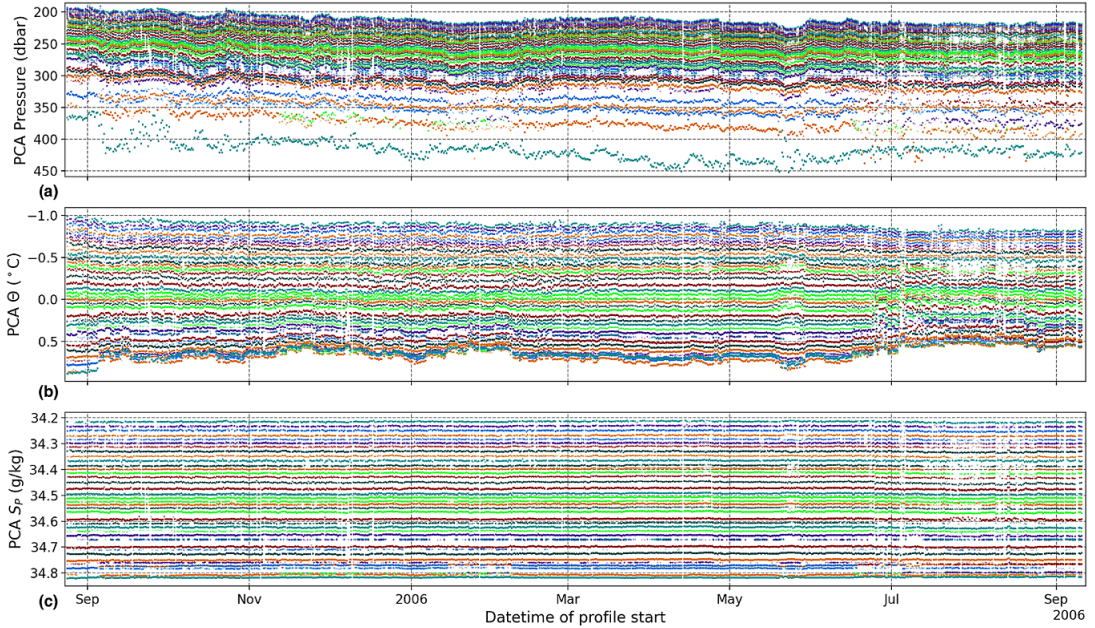
Figure 4. *The average (a) pressure, (b) Θ, and (c) S_P for the points within each cluster for each profile (profile cluster average, PCA) across time. The clustering algorithm was run with $m_{pts} = 580$ and $\ell = 25$ dbar on 678,575 data points in the salinity range of 34.21–34.82 g/kg from all up-going ITP3 profiles.*

Table 3. *The median normalized inter-cluster ranges and differences between average values of adjacent clusters for ITP2 and ITP3 calculated after removing outliers with z-score > 2 in the respective variable*

	$\widehat{IR}_{\mathrm{p}}$	$\widehat{IR}_{\Theta}$	$\widehat{IR}_{S_P}$	$\widehat{\Delta\Theta}$ (°C)	$\widehat{\Delta S_P}$ (mg/kg)
ITP2	8.394	4.087	0.707	0.048	16.5
ITP3	16.641	7.141	0.927	0.050	15.4

layers, which is a well-known phenomenon (Neshyba et al., 1972; Padman and Dillon, 1988; Kimura et al., 2015).

We can learn more about these features from the illustrative sets of particular salinity profiles from ITP2 presented in Figure 6. Both sets of profiles span less than a week, and we narrow the displayed pressure ranges so that the individual steps are visible. This figure shows that, overall, the algorithm captures the layered structure very well, marking points within interfaces as noise. Nevertheless, it is imperfect. Near layer boundaries, the algorithm sometimes includes points from an interface within a cluster, and sometimes neglects to include points within a layer. Additionally, as seen in the first profile of Figure 6(b) around 236 dbar, the algorithm can also miss layers entirely, especially when the layer is particularly thin and only present in a small number of profiles. Occasional issues such as these are to be expected with any automated detection method.

Focusing on ITP2 as an example, we find two outliers in IR_{S_P} marked by an orange 4-pointed star and a green " × " in Figure 5(a). We can track the same clusters in Figure 2(c), indicated by orange or green dots with a 4-pointed star or a " × " at the center of the cluster. They both have an average $S_P \approx 34.67$ g/kg but are separated in Θ'. A series of individual salinity profiles associated with these outliers over approximately 6 days is shown in Figure 6(a). We find that these outliers correspond to a relatively thick single
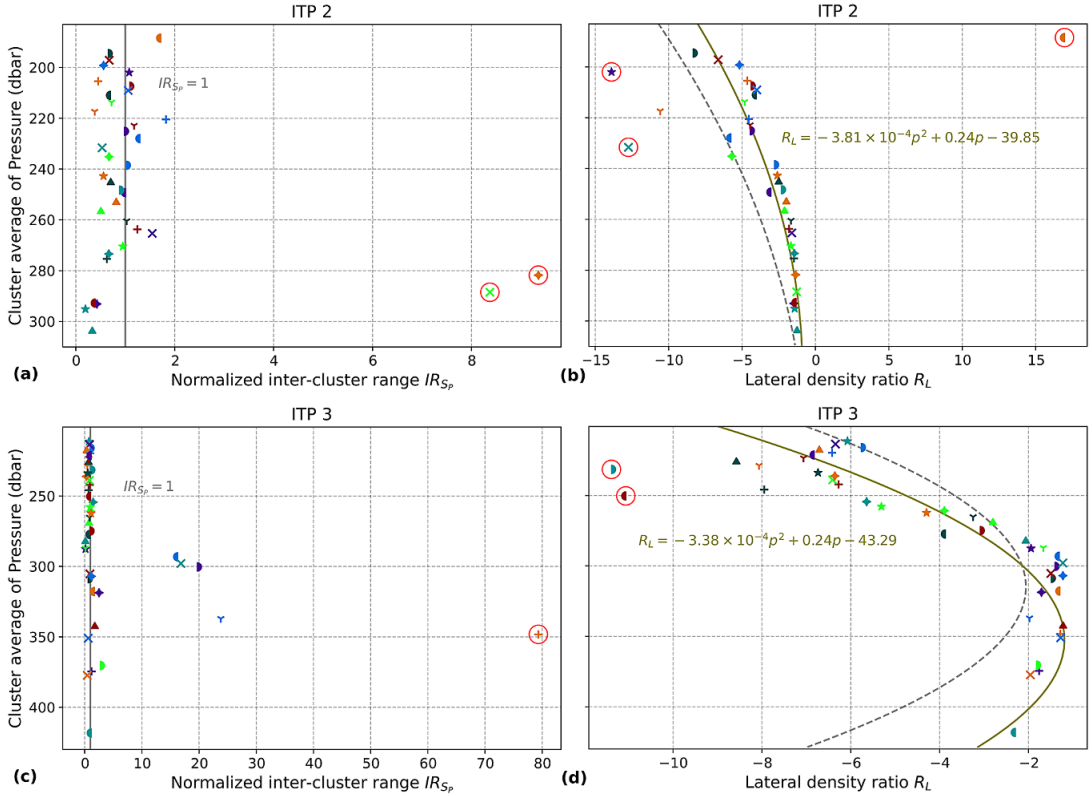
Figure 5. *The value of each cluster's normalized inter-cluster range for salinity IR_{S_P} in (a) and (c) and the lateral density ratio R_L in (b) and (d) as a function of the cluster's average pressure. The colors and markers for ITP2 in (a) and (b) are the same as the clustering shown in Figure 2 and for ITP3 in (c) and (d), they are the same as shown in Figure 4. Markers circled in red indicate outliers with a z-score greater than 2. (b) The solid curve is a second-degree polynomial fit (equation given by the annotation) for the non-outlier points from ITP2 and the dashed curve is the same for ITP3. (d) The solid curve is a second-degree polynomial fit (equation given by the annotation) for the non-outlier points from ITP3, and the dashed curve is the same for ITP2.*

layer that was erroneously split across two clusters by the algorithm. We attribute this erroneous splitting to the zig-zag pattern in $\Theta'-S_P$ space mentioned in Section 3.2 and note that it could be eliminated with a different selection of ℓ. Although we can attribute these outliers in IR_{S_P} to an artifact of the method, there are other instances where such outliers indicate the presence of physical features, as we will discuss in Section 4.3.

Next, we examine outliers in R_L, defined in Equation (3.2), for ITP2, marked by red circles in Figure 5(b). These outliers correspond to clusters that appear to have multiple layers grouped together. For example, the outlier cluster marked by an orange half-circle in Figure 5(b) can be seen in Figure 2(c) spanning $S_P = 34.054$–34.159, a much wider range than any other cluster. Similarly, in Figure 2(c), the outlier cluster marked by a purple star spans $S_P = 34.233$–34.261 and clearly encompasses what should be two distinct clusters. Some outliers in R_L are the result of erroneously clustering multiple layers together. On the other hand, the particular feature of the outlier cluster marked by a teal "$\times$," centered around 232 dbar with $R_L = -12.7$ in Figure 5(b), indicates splitting or merging. As highlighted in Figure 6(b), it typically spans multiple stair steps, but in the last few profiles, it only spans a single, larger step. This illustrates that we can use outliers in R_L to identify clusters that are not single, complete layers and to find instances of potential splitting or merging.
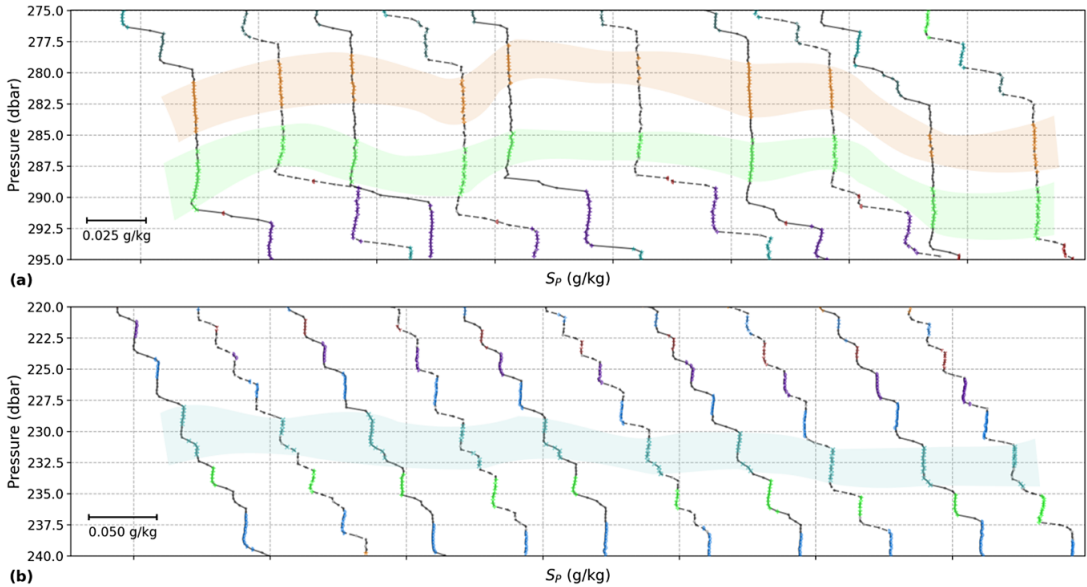
Figure 6. *Individual S_P profiles from ITP2, specifically chosen to show the examples of outlier clusters in IR_{S_P} and R_L highlighted by the bands of color. (a) Profiles 67, 69, 73, 75, 81, 83, 91, 93, 97, and 99 collected between August 31 and September 5, 2004. (b) Profiles 87, 89, 95, 97, 99, 101, 103, 105, 109, and 111 collected between September 3 and 7, 2004. The colors and markers are the same as the clustering shown in Figure 2. The gray dots are noise points, and the black lines show the profiles. Each profile is offset in S_P for clarity.*

4.3. Remnant intrusions revealed by temperature

Direct comparisons with other layer detection methods can also be used to identify interesting physical features. To demonstrate this, here we directly compare average layer characteristics computed by HDBSCAN to those reported by L22, both using data from ITP3. L22 used 758 profiles from ITP3, while we used all 766 available up-going profiles. Based on the gaps in Figure 3 of L22, we believe that the eight missing up-going profiles are from July 2006. Figure 7 shows the average Θ and S_P for each cluster found in our study and by L22 based on the values in their Table A1 after converting θ to Θ. We initially find 43 clusters and, after eliminating outliers in IR_{S_P} and R_L as described in Section 3.3, we find 40 clusters. While L22 identified only 34 thermohaline layers, we find close agreement between those and the clusters we found for $S_P \lesssim 34.74$ g/kg. Below where this salinity occurs in the water column, we find five more clusters than L22.

The differences between these two results appear to be related to the presence of *remnant intrusions*, which display features of both staircase layers and intrusions and are thought to represent an intermediate stage in staircase formation. Such features are known to appear near the bottom of staircases around the AW core and have been analyzed in detail by Bebieva and Timmermans (2019). They are characterized by homogeneous salinity, which leads the method of L22 to treat them as single layers. However, they have a temperature structure that is inverted (warmer above colder) compared to the typical gradient within a thermohaline staircase. The warm and cold sections are distinct enough for the clustering algorithm to split the structure into multiple clusters, each of which is homogeneous in salinity and relatively homogeneous in temperature. Figure 8 highlights an example of a remnant intrusion where the method of L22 gives results that differ from ours; the layer spanning approximately 320–340 dbar is constant in S_P, but decreases in Θ with depth and is divided into two clusters using the clustering method. These two clusters can be found in Figure 5(c), indicated by the blue "Y" centered around 337 dbar with $IR_{S_P} = 23.8$ and the orange "+" centered around 348 dbar with $IR_{S_P} = 79.3$.
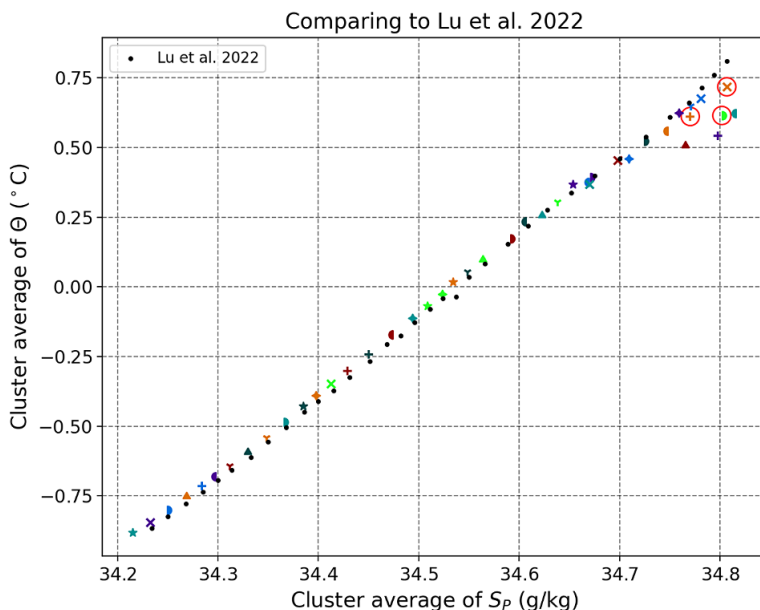
Figure 7. *The average Θ and S_P for the 34 layers found by Lu et al. (2022) in black dots and for the 43 layers found in our study using data from ITP3 and the same colors and markers as in Figure 4. Clusters circled in red are outliers in either IR_{S_P} or R_L.*
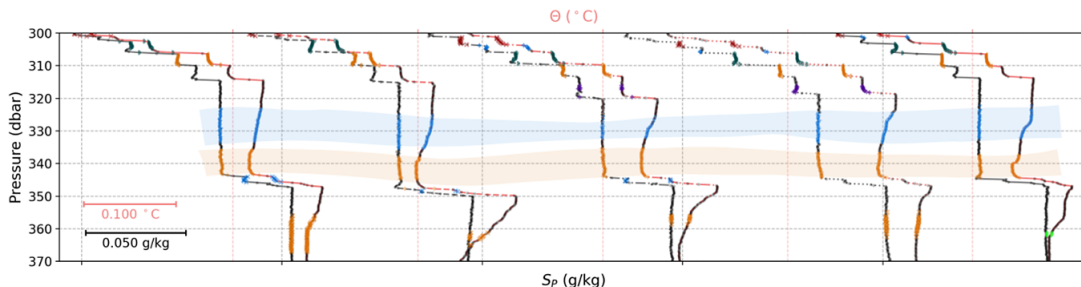

Figure 8. *Individual profiles 313, 315, 317, 319, and 321 from ITP3, collected between November 10 and 12, 2005, specifically chosen to show the example of a temperature inversion highlighted by the bands of color. The colors and markers of the individual points are the same as the clustering shown in Figures 4 and 7. The gray dots are noise points. The black lines on the left of each pair are the S_P profiles, while the red lines on the right are for Θ. Each profile is offset in both S_P and Θ for clarity.*

Such remnant intrusions exist between the active intrusions of the AW core and the staircase layers of the LHW. Staircases may be formed from intrusions, but such features have distinctly different patterns of heat and salt flux from double-diffusively driven staircases (Bebieva and Timmermans, 2019). The disagreement between our results and those of L22 highlights the difficulty of detecting remnant intrusions. While neither method is designed to automatically distinguish between these and staircase layers, the method presented here offers the opportunity to identify them when evaluating outlier clusters. Moreover, although Table 3 supports the suggestion by L22 that salinity is the most appropriate variable by which to identify staircase layers, having shown that a layer identified by L22 is, in fact, a remnant intrusion illustrates why it remains important to consider temperature as well.

4.4. Dependence of R_L on pressure

Lastly, we revisit Figure 5(b,d), where the distribution of points suggests a dependence of R_L on pressure. This is in contrast to previous studies which have found a constant R_L for the depth range we analyze (Timmermans et al., 2008; Toole et al., 2011; Bebieva and Timmermans, 2019). For ITP2 in panel (b), after removing the five outliers indicated across panels (a) and (b), we use a second-degree polynomial fit to find $R_L = -3.81 \times 10^{-4}p^2 + 0.24p - 39.85$, where p is pressure, with a coefficient of determination $R^2 = 0.67$. For ITP3 in panel (d), we remove the three outliers in panels (c) and (d), and then find quite a similar dependence of $R_L = -3.38 \times 10^{-4}p^2 + 0.24p - 43.29$ with a coefficient of determination $R^2 = 0.84$. Comparing these two curves in Figure 5(b,d), we find most of the difference can be explained by a downward shift of roughly 20 dbar in the upper water column to 50 dbar in the lower water column from ITP2 to ITP3. Note that a second-degree polynomial was chosen here as a simple parametric model to capture the apparent non-linear dependence of that R_L on pressure.

By contrast, T08 concluded there was no vertical dependence of R_L. They analyzed data from ITP1 through ITP6, which sampled the Canada Basin during the period from 2004 to 2007, and found a constant value of $R_L = -3.7 \pm 0.9$. Their Figure 6(a) shows five values of R_L for ITP2 that range from -3.5 to -3.0. While Bebieva and Timmermans (2019) found that R_L changes below the depth of the temperature maximum, those authors also found in their Figure 3(b) that R_L is constant in the depth range we consider in this study. Additionally, the presence of remnant intrusions does not explain the difference in our results, as the pressure dependence of R_L is evident in the upper part of the water column where they are absent. Although we find that R_L depends on pressure, our results agree with those of T08 on the magnitude of R_L, as we find the mean value for all non-outlier clusters of ITP2 to be -3.55 with a standard deviation of 2.24, and so we compare more of our results to those of T08.

We reproduce several of the figures from T08 in Figure 2. The combinations of color and markers for the clusters are the same in Figures 2, 5, and 6. In Figure 2(a), we plot data from ITP2 in Θ–S_P space, reproducing Figure 5(a) from T08. Those authors noted that points from each particular layer clustered along lines in Θ–S_P space that cross isopycnals, and when we mark the clusters found by the algorithm, those layers become visually distinct. Figure 2(b) shows profile 185 in the same depth range as Figure 4 from T08, plus the up-going profiles taken by ITP2 immediately before and after. This illustrates that the clustering algorithm is indeed marking points within those particular layers as in the same cluster and points within interfaces as noise. It also shows that the clustering algorithm tracks the same layers across neighboring profiles even though the pressure at which those layers are found varies. Figure 2(c) shows the ITP2 data on the axes used by the clustering algorithm. In Figure 2(d), we plot the clusters bounded by the box in Figure 2(a) in $\alpha\Theta$–βS_P space, reproducing Figure 6(a) from T08. The dashed lines of slope 1 correspond to isopycnals as $\Delta\rho = -\alpha\Delta\Theta + \beta S_P$. Overall, the panels in Figure 2 are close visual matches for those particular figures in T08.

After examining the differences between the two in detail (see Supplementary Material), it remains unclear why the values of R_L we found for clusters in ITP2 data differ from T08. However, we believe that the quantitative agreement in magnitude for the values of R_L and the qualitative match between the clustering results and the features in Figure 2 show that the clustering method reproduces those results from T08. Overall, these findings suggest that the clustering algorithm is indeed revealing a dependence of R_L on pressure in the data we analyzed from ITP2 and ITP3. Since R_L is directly related to the ratio of the vertical derivatives of the vertical fluxes of salinity and heat within a staircase (Bebieva and Timmermans, 2019), this could indicate a pressure dependence of that ratio.

5. Discussion

In this paper, we have presented a method based on the HDBSCAN clustering algorithm to both detect and connect well-mixed layers in thermohaline staircases across Arctic Ocean hydrographic data. HDBSCAN has previously been successfully applied to sets with millions of data points (Logan and Fotopoulou, 2020). As the comparison with results from previous studies was favorable, this suggests that this method

may produce trustworthy results when applied to datasets with larger numbers of points. This study contributes to a growing set of examples of clustering algorithms being used in oceanography (e.g., Koszalka and LaCasce, 2010; Espejo et al., 2014; Maze et al., 2017; Jones et al., 2019; Ma et al., 2019; Houghton and Wilson, 2020; Rosso et al., 2020, Desbruyères et al., 2021, Sonnewald et al., 2021). The continued and extended use of clustering algorithms in oceanography and related fields is an important development since discovering and detecting features in all manner of datasets becomes more challenging as they grow ever larger.

Special attention was given herein to the identification of outliers using parameters output by the method itself. We found that clusters which are outliers in the lateral density ratio R_L often indicate multiple layers that are erroneously clustered together, but can also highlight potential instances of layer splitting or merging. By introducing the normalized inter-cluster range IR_v, we quantitatively showed that the pressure and temperature values vary more within a layer than the difference between the values of neighboring layers, while the opposite is true for salinity. Because we know that the practical salinity S_P values in a particular layer are well separated from those of neighboring layers, we identified clusters with notably large values of IR_{S_P} as likely to be either only part of a layer that was erroneously split by the algorithm or a remnant intrusion. This study also suggests that there may be a pressure dependence of the lateral density ratio R_L, seen in both ITP2 and ITP3. The reasons for this dependence are unclear and are worthy of further study. Following the model presented by Bebieva and Timmermans (2019), the ratio of vertical fluxes of heat and salt could be recalculated using this more complex vertical dependence of R_L. This could then be compared to simulations (Yang et al., 2022) and parameterizations (Radko et al., 2014; Shibley and Timmermans, 2019) of the flux ratio in other models. However, in order to verify these with observations, vertical resolution fine enough to resolve the interfaces between layers, that is, finer than provided by ITPs, would be needed.

The method we presented here has certain advantages in particular circumstances. For example, all of the other methods referred to herein (Timmermans et al., 2008; Shibley et al., 2017; van der Boog et al., 2021b; Lu et al., 2022) require setting one or multiple thresholds on gradients in temperature, salinity, or density which are used to identify sections of profiles where layers may be present. However, choosing reasonable values for these thresholds requires precise prior knowledge of the staircase properties, which may not be available before identifying staircases in that particular region and time period. The method presented here requires the selection of a salinity range in which to search and an estimate of the typical layer thickness, which can be determined from a brief look at a dataset or from previous studies. To evaluate the clusters, a selection of an outlier detection method is required. In addition, while the other techniques require resolution high enough to resolve small-scale vertical gradients, the method presented here—which does not distinguish between individual profiles—only requires that a sufficient number of data points be available in order to detect clusters. Therefore, this technique could potentially find staircases in datasets that have too low a resolution to resolve the steps in any particular profile. While, in this study, we use all data points available after filtering, we found that subsampling profiles to every second, third, or fourth point yielded similar results (not shown). Finally, the method automatically connects layers across profiles. While L22 used an automated connection method, it still required subsequent adjustments to the layers to be made manually. Consequently, the method presented here could be readily applied to datasets with larger numbers of points and used to examine the large-scale, lateral properties of coherent layers in thermohaline staircases.

The clustering algorithm has several limitations. It cannot be used to examine sets of profiles spanning temporal or spatial scales larger than those on which stairs are known to be coherent. This method considers all profiles simultaneously, and it is not applicable to identifying stair steps in datasets of independent individual profiles. While this method could be applied on a profile-by-profile basis, each profile would require a separate selection of m_{pts}, which itself becomes highly sensitive with a small number of points to cluster. Moreover, as the clustering algorithm does not consider profiles individually, it may miss layers that are only present in a small number of profiles, as may occur especially for layers that split or merge. Finally, although the clustering method captures the overall structure of the staircase

layers well, it sometimes miscategorizes points, especially near the boundaries between layers and interfaces.

The method presented here could be used in conjunction with other staircase detection methods. For example, if a different detection method were used to identify which data points in a collection of profiles are in layers, the clustering algorithm could be run on just the layer points to automatically connect the layers across profiles. Additionally, the clustering algorithm could be used on a large collection of datasets to identify which subsets contain staircases; then, a more specifically tuned staircase detection method could be used on just that subset, reducing the amount of time-consuming analysis.

Because the method can be scaled to datasets with a larger number of points, a natural extension would be to apply it to a dataset with profiles from many ITPs. Furthermore, although we have focused on identifying upper-ocean Arctic thermohaline staircases, it could also be useful in other oceanic regimes. Staircases with steps on the order of 50 m thick have been observed in the Arctic between depths of 2000–3000 m (Timmermans et al., 2003), much deeper than ITPs measure, while the Argo network of autonomous profiling floats has captured staircases in regions all over the world (van der Boog et al., 2021a). Since this method does not assume a consistent vertical resolution across the profiles, it could be run on a mix of data from different types of instruments, assuming they operated within the same region and time period. This method could also be adjusted to identify other structures that appear in Θ–S space, such as different types of layers or water masses, or even structures that can appear in different spaces, such as Θ–O_2 (Rosso et al., 2020). On the technical side, another topic of future study would be to adapt this method to automatically distinguish between well-mixed layers and intrusions. However, when using this clustering algorithm to specifically search for staircase layers, we recommend avoiding the bottom of the thermocline around the AW core, where remnant intrusions are known to appear (Bebieva and Timmermans, 2019). Finally, there may be methods other than the DBCV validation process used herein that may be better able to guide the choice of parameters, potentially improving the detection fidelity.

Author contribution. Conceptualization: M.G.S., N.G., E.R., J.M.L.; data curation: M.G.S.; formal analysis: M.G.S.; funding acquisition: N.G.; investigation: M.G.S.; methodology: M.G.S.; software: M.G.S.; supervision: N.G., E.R., J.M.L.; validation: M.G.S., N.G., E.R., J.M.L.; visualization: M.G.S.; writing – original draft: M.G.S.; writing – review & editing: M.G.S., N.G., E.R., J.M.L.; All authors approved the final submitted draft.

References

André Q, **Barker AJ and Mathis S** (2017) Layered semi-convection and tides in giant planet interiors. *Astronomy & Astrophysics* *605*, A117. https://doi.org/10.1051/0004-6361/201730765.

Bebieva Y and Timmermans ML (2019) Double-diffusive layering in the Canada Basin: An explanation of a long-layer temperature and salinity gradients. *Journal of Geophysical Research: Oceans 124*(1), 723–735. https://doi.org/10.1029/2018JC014368.

Campello RJGB, **Moulavi D and Sander J** (2013) Density-based clustering based on hierarchical density estimates. *Lecture Notes in Computer Science 7819*, 160–172. https://doi.org/10.1007/978-3-642-37456-2_14.

Carmack EC (2007) The alpha/beta ocean distinction: A perspective on freshwater fluxes, convection, nutrients and productivity in high-latitude seas. *Deep-Sea Research Part II: Topical Studies in Oceanography 54*(23–26), 2578–2598. https://doi.org/10.1016/j.dsr2.2007.08.018.

Chen LG (1995) Mixed layer density ratio from the Levitus data. *Journal of Physical Oceanography 25*(4), 691–701. https://doi.org/10.1175/1520-0485(1995)025<0691:MLDRFT>2.0.CO;2.

Comiso JC, **Parkinson CL**, **Gersten R and Stock L** (2008) Accelerated decline in the Arctic Sea ice cover. *Geophysical Research Letters 35*(1), 1–6. https://doi.org/10.1029/2007GL031972.

Desbruyères D, **Chafik L and Maze G** (2021) A shift in the ocean circulation has warmed the subpolar North Atlantic Ocean since 2016. *Communications Earth & Environment 2*(1). https://doi.org/10.1038/s43247-021-00120-y.

Espejo A, **Camus P**, **Losada IJ and Méndez FJ** (2014) Spectral Ocean wave climate variability based on atmospheric circulation patterns. *Journal of Physical Oceanography 44*(8), 2139–2152. https://doi.org/10.1175/JPO-D-13-0276.1.

Ester, M., **Kriegel, H.-P.**, **Sander, J.**, & **Xu, X.** (1996). A Density-Based Algorithm for Discovering Clusters in Large Spatial Databases with Noise. In *Proceedings of the Second International Conference on Knowledge Discovery and Data Mining*. Amsterdam, Netherlands: Elsevier, pp. 226–231.

Hinneburg A and Keim DA (2003) A general approach to clustering in large databases with noise. *Knowledge and Information Systems 5*(4), 387–415. https://doi.org/10.1007/s10115-003-0086-9.

Houghton IA and Wilson JD (2020) El Niño detection via unsupervised clustering of Argo temperature profiles. *Journal of Geophysical Research: Oceans 125*(9), 1–12. https://doi.org/10.1029/2019JC015947.

Jones DC, **Holt HJ**, **Meijers AJ and Shuckburgh E** (2019) Unsupervised clustering of Southern Ocean Argo float temperature profiles. *Journal of Geophysical Research: Oceans 124*(1), 390–402. https://doi.org/10.1029/2018JC014629.

Kimura S, **Nicholls KW and Venables E** (2015) Estimation of ice shelf melt rate in the presence of a thermohaline staircase. *Journal of Physical Oceanography 45*(1), 133–148. https://doi.org/10.1175/JPO-D-14-0106.1.

Koszalka IM and LaCasce JH (2010) Lagrangian analysis by clustering. *Ocean Dynamics 60*(4), 957–972. https://doi.org/10.1007/s10236-010-0306-2.

Krishfield R, **Toole J and Timmermans M** (2008) *ITP Data Processing Procedures*. Woods Hole Oceanographic Institution, pp. 1–24.

Logan CHA and Fotopoulou S (2020) Unsupervised star, galaxy, QSO classification. *Astronomy & Astrophysics 633*, A154. https://doi.org/10.1051/0004-6361/201936648.

Lu Y-Z, **Guo S-X**, **Zhou S-Q**, **Song X-L and Huang P-Q** (2022) Identification of thermohaline sheet and its spatial structure in the Canada Basin. *Journal of Physical Oceanography 52*(11), 2773–2787. https://doi.org/10.1175/JPO-D-22-0012.1.

Ma C, **Li S**, **Yang Y**, **Yang J and Chen G** (2019) Extraction of revolving channels of drifters around mesoscale Eddy Centers based on spatiotemporal trajectory clustering. *Journal of Atmospheric and Oceanic Technology 36*(9), 1903–1916. https://doi.org/10.1175/JTECH-D-19-0007.1.

Maykut GA and Untersteiner N (1971) Some results from a time-dependent thermodynamic model of sea ice. *Journal of Geophysical Research 76*(6), 1550–1575. https://doi.org/10.1029/jc076i006p01550.

Maze G, et al. (2017) Coherent heat patterns revealed by unsupervised classification of Argo temperature profiles in the North Atlantic Ocean. *Progress in Oceanography 151*, 275–292. https://doi.org/10.1016/j.pocean.2016.12.008.

McDougall TJ and Barker PM (2011). Getting started with TEOS-10 and the Gibbs Seawater (GSW) Oceanographic Toolbox. 3.06.12 edition. Available at www.TEOS-10.org (accessed 9 March 2023).

McInnes L, **Healy J and Astels S** (2017) hdbscan: Hierarchical density based clustering. *Journal of Open Source Software*, *2*(11), 205, https://doi.org/10.21105/joss.00205.

Ménesguen C, **Lique C and Caspar-Cohen Z** (2022) Density staircases are disappearing in the Canada Basin of the Arctic Ocean. *Journal of Geophysical Research: Oceans 127*(11). https://doi.org/10.1029/2022JC018877.

Moulavi D, **Jaskowiak PA**, **Campello RJGB**, **Zimek A and Sander J** (2014) Density-based clustering validation. In *Proceedings of the 2014 SIAM International Conference on Data Mining*. Philadelphia, PA: Society for Industrial and Applied Mathematics, vol. *2*, pp. 839–847. https://epubs.siam.org/doi/10.1137/1.9781611973440.96.

Neal VT and Neshyba S (1973) Microstructure anomalies in the Arctic Ocean. *Journal of Geophysical Research 78*(15), 2695–2701. https://doi.org/10.1029/JC078i015p02695.

Neal VT, **Neshyba S and Denner W** (1969) Thermal stratification in the Arctic Ocean. *Science 166*(3903), 373–374. https://doi.org/10.1126/science.166.3903.373.

Neshyba S, **Neal VT and Denner W** (1971) Temperature and conductivity measurements under Ice Island T-3. *Journal of Geophysical Research 76*(33), 8107–8120. https://doi.org/10.1029/JC076i033p08107.

Neshyba S, **Neal VT and Denner WW** (1972) Spectra of internal waves: In-situ measurements in a multiple-layered structure. *Journal of Physical Oceanography 2*(1), 91–95. https://doi.org/10.1175/1520-0485(1972)002<0091:SOIWSM>2.0.CO;2.

Newman FC (1976) Temperature steps in Lake Kivu: A bottom heated saline Lake. *Journal of Physical Oceanography 6*(2), 157–163. https://doi.org/10.1175/1520-0485(1976)006<0157:TSILKA>2.0.CO2.

Padman L and Dillon TM (1987) Vertical heat fluxes through the Beaufort Sea thermohaline staircase. *Journal of Geophysical Research 92*(C10), 10799. https://doi.org/10.1029/JC092iC10p10799.

Padman L and Dillon TM (1988) On the horizontal extent of the Canada Basin thermohaline steps. *Journal of Physical Oceanography 18*(10), 1458–1462. https://doi.org/10.1175/1520-0485(1988)018<1458:OTHEOT>2.0.CO;2.

Padman L and Dillon TM (1989) Thermal microstructure and internal waves in the Canada Basin diffusive staircase. *Deep Sea Research Part A, Oceanographic Research Papers 36*(4), 531–542. https://doi.org/10.1016/0198-0149(89)90004-6.

Peralta-Ferriz C and Woodgate RA (2015) Seasonal and interannual variability of pan-Arctic surface mixed layer properties from 1979 to 2012 from hydrographic data, and the dominance of stratification for multiyear mixed layer depth shoaling. *Progress in Oceanography 134*, 19–53. https://doi.org/10.1016/j.pocean.2014.12.005.

Pontin CM, Barker AJ, Hollerbach R, André Q and Mathis S (2021) Wave propagation in semiconvective regions of giant planets. *Monthly Notices of the Royal Astronomical Society 493*(4), 5788–5806. https://doi.org/10.1093/mnras/staa664.

Radko T (2013) *Double-Diffusive Convection*. Cambridge University Press. https://doi.org/10.1017/CBO9781139034173.

Radko T, Bulters A, Flanagan JD and Campin JM (2014) Double-diffusive recipes. Part I: Large-scale dynamics of thermohaline staircases. *Journal of Physical Oceanography 44*(5), 1269–1284. https://doi.org/10.1175/JPO-D-13-0155.1.

Rosso I, Mazloff MR, Talley LD, Purkey SG, Freeman NM and Maze G (2020) Water mass and biogeochemical variability in the Kerguelen sector of the Southern Ocean: A machine learning approach for a mixing hot spot. *Journal of Geophysical Research: Oceans 125*(3), 1–23. https://doi.org/10.1029/2019JC015877.

Schmitt R, Perkins H, Boyd J and Stalcup M (1987) C-SALT: An investigation of the thermohaline staircase in the western tropical North Atlantic. *Deep Sea Research Part A. Oceanographic Research Papers 34*(10), 1655–1665. https://doi.org/10.1016/0198-0149(87)90014-8.

Shaw WJ and Stanton TP (2014) Vertical diffusivity of the Western Arctic Ocean halocline. *Journal of Geophysical Research: Oceans 119*(8), 5017–5038. https://doi.org/10.1002/2013JC009598.

Shibley NC and Timmermans M-L (2019) The formation of double-diffusive layers in a weakly turbulent environment. *Journal of Geophysical Research: Oceans*. https://doi.org/10.1029/2018JC014625.

Shibley NC, Timmermans M-L, Carpenter JR and Toole JM (2017) Spatial variability of the Arctic Ocean's double-diffusive staircase. *Journal of Geophysical Research: Oceans 122*(2), 980–994. https://doi.org/10.1002/2016JC012419.

Shibley NC, Timmermans ML and Stranne C (2020) Analysis of acoustic observations of double-diffusive Finestructure in the Arctic Ocean. *Geophysical Research Letters 47*(18), 1–11. https://doi.org/10.1029/2020GL089845.

Sonnewald M, Lguensat R, Jones DC, Dueben PD, Brajard J and Balaji V (2021) Bridging observations, theory and numerical simulation of the ocean using machine learning. *Environmental Research Letters 16*(7), 073008. https://doi.org/10.1088/1748-9326/ac0eb0.

Stewart KD and Haine TW (2016) Thermobaricity in the transition zones between alpha and beta oceans. *Journal of Physical Oceanography 46*(6), 1805–1821. https://doi.org/10.1175/JPO-D-16-0017.1.

Stranne C, Mayer L, Weber TC, Ruddick BR, Jakobsson M, Jerram K, Weidner E, Nilsson J and Gårdfeldt K (2017) Acoustic mapping of thermohaline staircases in the Arctic Ocean. *Scientific Reports 7*(1), 1–9. https://doi.org/10.1038/s41598-017-15486-3.

Timmermans M-l, Garrett C and Carmack E (2003) The thermohaline structure and evolution of the deep waters in the Canada Basin, Arctic Ocean. *Deep Sea Research Part I: Oceanographic Research Papers 50*, 1305–1321. https://doi.org/10.1016/S0967-0637(03)00125-0.

Timmermans M-L, Toole J, Krishfield R and Winsor P (2008) Ice-tethered profiler observations of the double-diffusive staircase in the Canada Basin thermocline. *Journal of Geophysical Research 113*, 1–10. https://doi.org/10.1029/2008jc004829.

Toole JM, Krishfield RA, Timmermans ML and Proshutinsky A (2011) The ice-tethered profiler: Argo of the Arctic. *Oceanography 24*(3), 126–135. https://doi.org/10.5670/oceanog.2011.64.

Turner JS (2010) The melting of ice in the Arctic Ocean: The influence of double-diffusive transport of heat from below. *Journal of Physical Oceanography 40*(1), 249–256. https://doi.org/10.1175/2009JPO4279.1.

van der Boog CG, Dijkstra HA, Pietrzak JD and Katsman CA (2021a) Double-diffusive mixing makes a small contribution to the global ocean circulation. *Communications Earth & Environment 2*(1), 46. https://doi.org/10.1038/s43247-021-00113-x.

van der Boog CG, Otto Koetsier J, Dijkstra HA, Pietrzak JD and Katsman CA (2021b) Global dataset of thermohaline staircases obtained from Argo floats and ice-tethered profilers. *Earth System Science Data 13*(1), 43–61. https://doi.org/10.5194/essd-13-43-2021.

Winton M (2011) Do climate models underestimate the sensitivity of northern Hemisphere Sea ice cover? *Journal of Climate 24*(15), 3924–3934. https://doi.org/10.1175/2011JCLI4146.1.

Yang Y, Verzicco R, Lohse D and Caulfield C (2022) Layering and vertical transport in sheared double-diffusive convection in the diffusive regime. *Journal of Fluid Mechanics 933*, A30. https://doi.org/10.1017/jfm.2021.1091.

Yu LS, Bosse A, Fer I, Orvik KA, Bruvik EM, Hessevik I and Kvalsund K (2017) The Lofoten Basin eddy: Three years of evolution as observed by Seagliders. *Journal of Geophysical Research: Oceans 122*(8), 6814–6834. https://doi.org/10.1002/2017JC012982.